On-the-go hyperspectral imaging for the in-field estimation of grape berry soluble solids and anthocyanin concentration

S. GUTIÉRREZ, J. TARDAGUILA, J. FERNÁNDEZ-NOVALES and M.P. DIAGO

Instituto de Ciencias de la Vid y del Vino (University of La Rioja, Consejo Superior de Investigaciones Científicas, Gobierno de La Rioja), 26007, Logroño, Spain

Corresponding author: Dr Maria-Paz Diago, email maria-paz.diago@unirioja.es

Abstract

Background and Aims: Hyperspectral imaging (HSI) is used to assess fruit composition mostly indoor under controlled conditions. This work evaluates a HSI technique to measure TSS and anthocyanin concentration in wine grapes non-destructively, in real time and in the vineyard.

Methods and Results: Hyperspectral images were acquired under natural illumination with a VIS–NIR hyperspectral camera (400–1000 nm) mounted on an all-terrain vehicle moving at 5 km/h in a commercial Tempranillo vineyard in La Rioja, Spain. Measurements were taken on four dates during grape ripening in 2017. Grape composition was analysed on the grapes imaged, which was then used to develop spectral models, trained with support vector machines, to predict TSS and anthocyanin concentration. Regression models of TSS had determination coefficients (R^2) of 0.91 for a fivefold cross validation [root mean squared error (RMSE) of 1.358°Brix] and 0.92 for the prediction of external samples (RMSE of 1.274°Brix). For anthocyanin concentration, R^2 of 0.72 for cross validation (RMSE of 0.282 mg/g berry) and 0.83 for prediction (RMSE of 0.211 mg/g berry) was achieved. Spatial–temporal variation maps were developed for the four image acquisition dates during ripening.

Conclusions: These results suggest that potential for on-the-go HSI to automate the assessment of important grape compositional parameters in vineyard is promising.

Significance of the Study: The on-the-go HSI method described in this study could be automated and provide valuable information to improve winery and vineyard decisions and vineyard management.

Keywords: *plant phenotyping, proximal sensing regression, sensors, support vector machines*

Introduction

Wine composition is affected by compounds present in grapes (Kennedy 2010). The monitoring of grape ripening is often based on measuring TSS and, in the case of red grapes, the anthocyanin concentration of berries. The TSS of grape berries is closely related to the fermentable sugar concentration and the alcohol concentration of the subsequent wine (Gomes et al. 2017). Anthocyanins are the pigmented phenolic substances present mostly in the skin of red grapes (Meléndez et al. 2013) responsible for red wine colour (Boulton 2001). These two grape compositional parameters are used to help determine harvest timing and are important for establishing grape prices in many wineries and cooperatives worldwide (Bramley et al. 2011). At present, methods for TSS and anthocyanin measurement in grapes are destructive, however, TSS can be quickly and easily measured using hand-held refractometers, but anthocyanin concentration analysis requires more time consuming wet chemistry methods (Iland et al. 2004, Liang et al. 2008). Therefore, it would be valuable for vineyards and wineries to have rapid, robust and non-destructive methods to assess TSS and anthocyanin concentration during grape ripening.

Furthermore, knowledge of the spatial–temporal variation of TSS and anthocyanin in fruit across a vineyard could inform better sampling, improve vineyard management and allow for selective harvesting. The pattern of spatial variability of grape anthocyanin in a Tempranillo vineyard changed with phenology (Baluja et al. 2012a,b), and, therefore, to obtain useful information it would be necessary to take measurements at different locations and at different times during ripening. This would require a large number of measurements. Unfortunately, rapid measurement of a large number of samples is not feasible for TSS or anthocyanin concentration.

Several studies have investigated manual in-field monitoring of grape composition (Ben Ghozlen et al. 2010, Baluja et al. 2012b, Barnaba et al. 2014), but the methods these studies are based on tend to be time consuming and labour intensive and, therefore, unsuitable for collecting large amounts of representative data. Remote sensing has been evaluated as a non-destructive alternative to assess the spatial variability of grape colour in the vineyard. Spectral indices, however, were weakly correlated with grape anthocyanin (Lamb et al. 2004). Other authors mounted a chlorophyll-based sensor above the discharge conveyor of a tow-behind harvester to measure the anthocyanin concentration of harvested fruit at georeferenced positions within the vineyard (Bramley et al. 2011). Although this enabled the mapping of spatial variability of grape anthocyanin, as the assessment was not completed until after the fruit was picked, there was no provision for selective harvesting.

Ground-based, on-the-go monitoring has the potential to replace manual data collection from the vineyard. This approach, however, does present challenges that have impeded its development and application (Ben Ghozlen et al. 2010). These challenges include: (i) the need for a sufficient amount of the fruit to be visible to the sensors; (ii) the small measuring area of many devices (e.g. ~3 cm^2,

doi: 10.1111/ajgw.12376

Fernández-Novales et al. (2017)) can make it difficult to image and sense enough fruit; (iii) the low signal to noise intensity of many devices monitoring; and (iv) the management and analysis of large data sets that may be generated.

Within the context of precision agriculture, the development of new sensors, especially with spectral capability, allows for the acquisition of high resolution data that could be useful for monitoring crop development. For instance, the ability to assess ripening rapidly, non-destructively and spatially would aid harvest decisions and provide objective information upon which to base selective harvesting.

In recent years, hyperspectral imaging (HSI) has gained prominence as a powerful technology for non-destructive analysis in several agricultural and food quality and safety applications (Sun 2010, Park and Lu 2015). Hyperspectral imaging combines two different fields: the potential of spectroscopy modelling with two-dimensional digital imaging. As each pixel in a hyperspectral image provides a full spectrum from the measured target, the capability of this technology for the extraction of information from the target is powerful. Hyperspectral imaging has been used to assess the chemical composition of fruit for a range of crops. Hyperspectral imaging-based modelling for predicting TSS has been studied in grape berries (Gomes et al. 2017, Piazzolla et al. 2017), apple (Ma et al. 2017, Mo et al. 2017, Tian et al. 2018) and mango (Rungpichayapichet et al. 2017), while HSI has also been used to predict the anthocyanin concentration in grape berries (Diago et al. 2016, Martínez-Sandoval et al. 2016, Zhang et al. 2017), mulberry (Huang et al. 2017) and raspberry (Rodríguez-Pulido et al. 2017). All these studies, however, were done in the laboratory and under controlled conditions, including controlled illumination, sample positioning and temperature. In the vineyard, ambient light and temperature as well as sample positioning are not constant and often difficult to predict. Consequently, although there are many potential applications for HSI in the field, there are also significant challenges to overcome. Thus, there are limited published studies on the use of in-field HSI (Deery et al. 2014, Williams et al. 2017). On-the-go approaches in robotics, however, have been reported (Underwood et al. 2017, Wendel and Underwood 2017). Given the demonstrated potential of HSI to assess grape composition, developing the technology to add on-the-go capability and mapping using automated platforms offers much promise.

Therefore, the goal of this study was to develop and evaluate non-destructive, in-field estimation and mapping of two important compositional parameters, namely TSS and the anthocyanin concentration, of berries using HSI.

Materials and methods

The study comprised three major stages (Figure 1). In stage one, the in-field experiments were conducted, involving on-the-go HSI image acquisition and collection and chemical analysis of the imaged grapes. In the second stage, the hyperspectral images were processed to automate the extraction of grape berry spectra and datasets collated. In the final stage, the data set was used to train different prediction models, using machine learning algorithms, and spatial–temporal maps were generated.

In-field experiments

Experimental layout. The experimental site was a 0.7 ha commercial vineyard Ábalos, La Rioja, Spain (latitude 42°34′45.7″, longitude −2°42′27.78″, asl 628 m). *Vitis vinifera* (L.) cultivar Tempranillo grapevines were planted in 2010, on rootstock R-110 and trained to a vertically shoot-positioned (VSP) trellis system. Rows were orientated northeast–southwest and row and vine spacing was 2.2 and 1.0 m, respectively. Three equal length rows were selected and within each row 12 blocks of 5 m containing five vines each were chosen for the spectral imaging and grape berry analysis. Hyperspectral images were acquired from the eastern side of the canopy, which was defoliated in the basal fruiting zone. In order to model relationships at various ripening stages, images were acquired on four dates between veraison and harvest. According to the modified Eichhorn and Lorenz system (Coombe 1995) these dates and stages during season 2017 were: 11 August, stage 36; 24 August, stage 37; 18 September, stage 38; and 28 September, stage 38. Therefore, the total number of five-vine blocks that were measured throughout the entire experiment was 144.

Hyperspectral images were acquired on-the-go using a push broom Resonon Pika L VNIR hyperspectral imaging camera (Resonon, Bozeman, MA, USA) that was installed on an all-terrain vehicle (ATV) (Trail Boss 330, Polaris Industries, MN, USA) (Figure 2) and connected to an industrial computer. The spectral resolution of the camera was 2.1 nm (300 bands from 400 to 1000 nm), with 300 pixels of spatial resolution. An 8 mm focal length lens was pointed to the canopy on a lateral point of view at 2.0 m of distance, casting a vertical recording line upon the plants of 1.32 m (field of view of 36.5°). The recording line covered the whole vine canopy, including the fruiting zone (Figure 2). The 36 measurements per day (one for each five-vine block) were performed on the south-eastern side of the canopy, between 1000 and 1400, under the natural illumination from the sun only. To test the HSI method under reproducible conditions (i.e. other types of terrestrial vehicles), no specific mechanical compensation was applied for terrain irregularity correction other than the suspension of the vehicle. Nevertheless, the distance between the camera and the vines ensured that the image acquired by the sensor always covered whole plants and, therefore, the grape bunches.

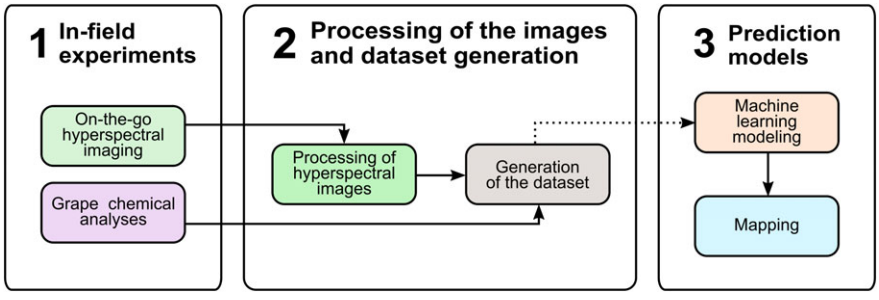

Figure 1. Design of the study, split into three major stages: in-field experiments, processing of the images and development of prediction models.

Figure 2. On-the-go hyperspectral imaging with a camera mounted on an all-terrain vehicle (ATV) at 5 km/h. Images of the entire vine canopy were obtained from the ATV's motion, by push-broom scanning, and used for the estimation of grape composition.

To take into account the variable illumination conditions, the values for the camera configuration parameters [integration time and frames per second (FPS)] were adapted for each block measurement, depending on the light intensity, in order to find the best trade-off between acceptable image composition, enough spectral intensity and the prevention of saturation. Frames per second ranged from 50 (taking one frame each 20 ms) at the beginning of the season to 40 at the end (one frame each 25 ms). Prior to the hyperspectral measurement, a Spectralon (Labsphere, Sutton, NH, USA) white reference (a surface with a reflectance over 95%) was manually presented to the camera simulating the same position and distance to the canopy of the fruit. A dark current measurement was conducted to obtain the inherent electronic noise. After this, the block was imaged on-the-go at a constant speed of 5 km/h, composing a hyperspectral image by push broom scanning (Figure 2) with an average number of scanlines (columns) of 710, with 900 pixels each one. On average, a total of 639 000 pixels (i.e. spectra) per block were acquired.

The spectral light intensity values collected by the camera were translated into reflectance (R) with the Equation 1:

$$R = \frac{G(\lambda) - D(\lambda)}{W(\lambda) - D(\lambda)} \quad (1)$$

where λ is a wavelength, G is the intensity of the light reflected by the canopy, W is the intensity of the light coming from the white reference, and D is the dark current. The reflectance was then converted into absorbance [$\log(1/R)$]. To prevent the noise that is commonly found in the tails of a spectral signal, the first ten bands and the last 50 were discarded, thus obtaining spectra that comprised 240 bands (from 410 to 921 nm).

Hyperspectral images were georeferenced using an Ag Leader 6500GPS receiver (Ag Leader Technology, Ames, IA, USA) with RTK correction installed on the ATV.

Analysis of grape composition. At each measurement date and immediately after the acquisition of HSI data for each five-vine block, exposed bunches were identified and 10–15 visible berries were removed and placed in labelled plastic bags for subsequent chemical analysis. On average, 200 grape berries per block were collected at each date. Berries were then transported, in portable refrigerators, to the laboratory and stored at −20°C until chemical analysis was completed.

Anthocyanin concentration and TSS of berries were measured. Berries were thawed overnight at 4°C before analysis. For each sample, a subsample of 100 randomly selected berries was hand crushed and filtered. The TSS was determined with a temperature compensating Quick-Brix 60 digital refractometer (Mettler Toledo, Columbus, OH, USA) and expressed as °Brix. The remaining berry subsample was homogenised with a T25 Ultra-Turrax high-performance disperser (IKA, Staufen, Germany) at high speed (14 000 rpm for 60 s). Anthocyanin concentration was then measured after Iland et al. (2004) and expressed as mg/g of berry.

Image processing

Processing of hyperspectral images. From each hyperspectral image, spectra belonging to grape bunches were obtained automatically. To do this, prior to image processing, a grape reference spectrum was obtained manually by selecting grape spectra from all the images (regions of approximately 200 spectra) and then averaging them. With this signature spectrum, pre-processed with a Saviztky–Golay smoothing and derivative (Savitzky and Golay 1964), the following described algorithm was coded using Python 3.6.1 (Free Software Foundation). Defining I as the original hyperspectral image and C as an empty matrix with the same width and height as I. Each one of the bins of C (with coordinates x, y) was filled with the determination coefficient from the correlation analysis between each one of the pixels of I in the same position (e.g. spectra in the x, y coordinates) and the grape signature spectra. The similarity of each pixel (spectrum) from I with the grape signature spectra was thus represented as an R^2 value, and a correlation matrix C was built. After a two-dimensional Gaussian smoothing to C (with σ set to 1.0), all the pixels from C that surpassed the 0.75 mark were identified as grape spectra and averaged (the 0.75 value was manually selected after intensive supervised review of the results of processing several hyperspectral images). This average was thus considered as the image (block) grape average spectrum. More details of this algorithm are presented in Table S1.

Figure 3 presents the output of this algorithm: (i) the original hyperspectral image is displayed with the red green blue (RGB) channels; (ii) the correlation matrix C after the Gaussian smoothing is shown; and (iii) the selected grape pixels (those from C whose R^2 is equal or greater than 0.75) are segmented.

In a small proportion of hyperspectral images, a limited number of pixels identified as grape had a spectral shape with higher intensity than that of the white reference. This was because of incident sunlight being directly reflected into the camera sensor and returning a reflectance value over 1.0 for some wavelengths. These pixels were discarded from final spectra averaging.

Generation of the data set. Grape berry spectra images and measurement of TSS and anthocyanin concentration for berries from each five-vine block comprised the data set, in which each spectrum was linked to corresponding compositional parameters. Combining 36 blocks and four measurement dates led to a data set comprising 144 samples. From

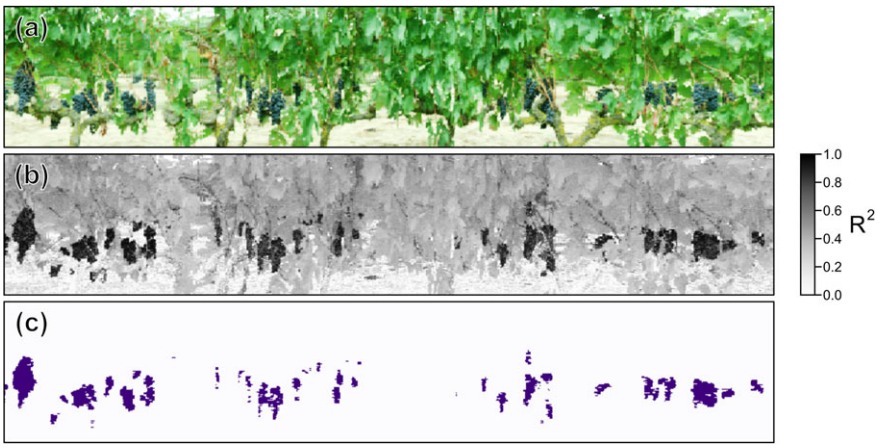

Figure 3. (a) Hyperspectral image from a block in red, green and blue (RGB) channels (histogram normalised for the sake of illustration). (b) Correlation matrix with R^2 values between the pixel spectrum and a grape reference spectrum. A Gaussian smoothing was applied with $\sigma = 1.0$. (c) Image with segmented grape pixels (pixels in (b) whose $R^2 \geq 0.75$). All the images were stretched in the horizontal axis for aesthetic purposes.

this, trained and tested subsets were built in an 80–20 ratio, respectively, by randomly extracting 20% of samples per date, making up a train set of 115 samples and a test set of 29 samples.

Development of prediction models

Machine learning modelling. Several machine learning algorithms were tested for modelling, based on the authors' experience and criteria. Epsilon-support vector machines (ε-SVMs) were chosen for training regression models because of superior performance. The input independent variable X was the spectra ($|X| = 240$, the number of spectral bands), pre-processed with standard normal variate (Barnes et al. 1989) and Savitzky–Golay filter (second-grade derivative, window size of 15), while the TSS and anthocyanin concentration were used as dependent variables y, each one for the training two different models. For TSS and anthocyanin concentration, a radial basis function kernel was used, with $\varepsilon = 0.1$ and $\gamma = 0.00417$ ($1/|X|$). The penalty parameter C was set to 100 in the case of TSS and to 30 for anthocyanin concentration. The performance of SVM for the train test was evaluated using a fivefold cross validation. The prediction results were obtained by training a model with all the samples from the train test and predicting the samples from the test set. All the models were developed using the Epsilon-support vector regression implementation in scikit-learn 0.18.1 (Pedregosa et al. 2011).

Spatial–temporal mapping. Interpolated TSS and anthocyanin concentration prediction maps were generated using multilevel b-spline interpolation (Lee et al. 1997) implemented in QGIS 2.19 (Free Software Foundation, Boston, MA, USA).

Results

Grape composition

The histograms for TSS and anthocyanin concentration on each experimental date are displayed in Figure 4. Berry TSS ranged from 10.7 to 25.2°Brix, indicating that many of the grapes reached maturity. Means and SDs indicated wide variability within measured TSS values. The results from anthocyanin analysis were similar to TSS, with values ranging from 0.05 (at veraison, when anthocyanin synthesis had yet to commence) to 2.01 mg/g berry at harvest. The mean values increased with ripening and the SD increased until September (EL stage 38).

With regard to the shape of the histograms for TSS and anthocyanin concentration, the gross of their values per date increased with ripening. For TSS, similar values were measured for the two last dates, indicating a final stage in maturity at which TSS in the berry had plateaued. In the case of anthocyanin concentration, the range increased with ripening, perhaps corresponding to asynchronous ripening of fruit.

Prediction models and mapping

The cross-validation and prediction results of the TSS models are shown in Figure 5. The fivefold cross validation (Figure 5a) yielded a determination coefficient R^2 of 0.91, with a root mean squared error (RMSE) of 1.358°Brix. The

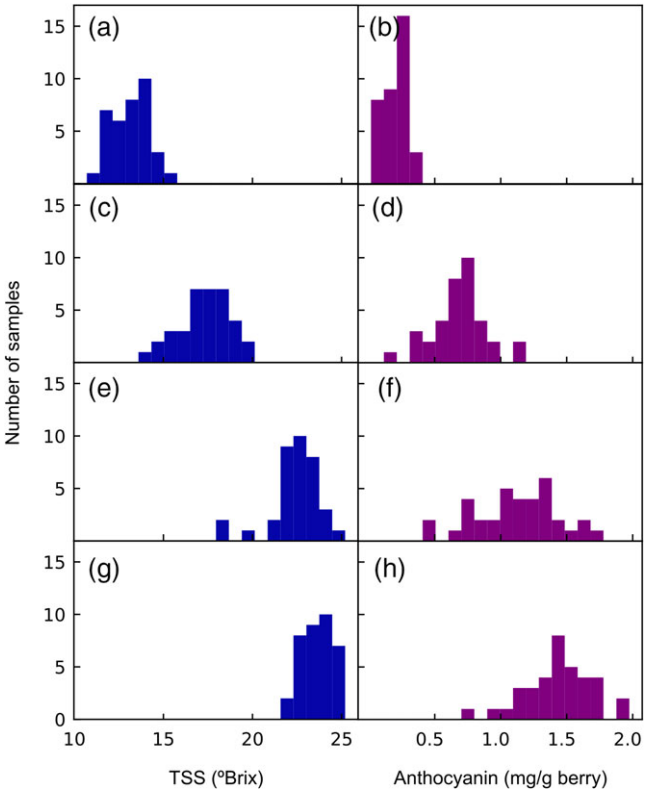

Figure 4. Histograms for (a, c, e, g) TSS and (b, d, f, h) anthocyanin concentration for (a, b) 11 August, (c, d) 24 August, (e, f) 18 September and (g, h) 28 September 2017. (a) Mean 13.08, SD 1.061; (b) mean 0.24, SD 0.090; (c) mean 17.27, SD 1.406; (d) mean 0.73, SD 0.199; (e) mean 22.44, SD 1.366; (f) mean 1.16, SD 0.315; (g) mean 23.57, SD 0.939; (h) mean 1.47, SD 0.268.

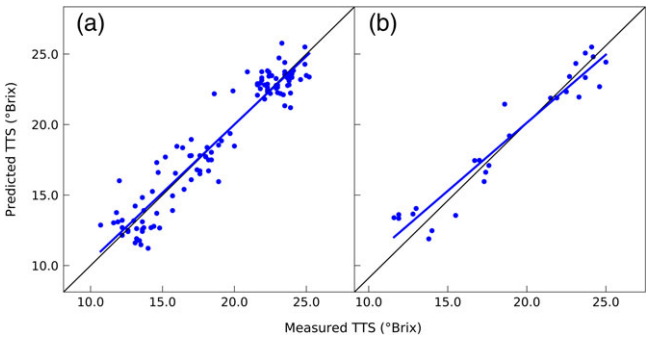

Figure 5. Regression plot for (a) fivefold cross validation (R^2 = 0.91; RMSE = 1.358) and (b) prediction results (R^2 = 0.92; RMSE = 1.274) for the TSS models, showing the regression line of the samples (——) and the 1:1 trend (——). RMSE, root mean squared error (in °Brix).

regression line was close to the 1:1 line with an even distribution of results. The prediction results (Figure 5b) cast comparable values for both R^2 (0.92) and RMSE (1.274°Brix).

Figure 6 shows the regression plots from cross validation and prediction models for berry anthocyanin concentration. Figure 6a displays a cross validation of R^2 of 0.72, while the prediction results (Figure 6b) yielded a larger determination coefficient of 0.83. For the first case, the RMSE value was 0.282 mg/g berry, but in Figure 6b the lower number of samples and their concentrated locations reduced the RMSE value to 0.211 mg/g berry.

In Figure 7, the evolution of TSS and anthocyanin concentration is displayed in eight prediction maps, one per date and grape composition parameter, for the vineyard. The accumulation of TSS (Figure 7) remained steady throughout the different maturity stages. Maximum values were reached in the latter stages of ripening but by the last sampling date there was only a slight increase in TSS. The south corner of the vineyard was the fastest to ripen.

In the case of the anthocyanin concentration, large differences were observed between the four dates, from little variation (from 0.15 to 0.35 mg/g berry) on 11 August, to a plot with higher anthocyanin concentration and variability on 28 September.

Computational cost

The processing of 36 hyperspectral images using the described algorithm took, per date, an average of 5 h and 35 min on an Intel Core i7-5820K CPU with 16 GB of RAM (Intel Corporation, Santa Clara, CA, USA) (no thread optimisation). Taking into account that each image was composed of approximately 710 scanlines (columns), the calculations resulted in an average processing time of 0.79 s per column, while the prediction of a single sample using a trained SVM model took 0.05 s. Thus, the processing and prediction of a hyperspectral scanline would take less than a second.

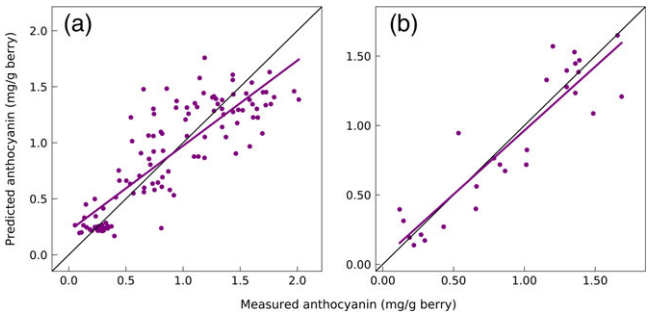

Figure 6. Regression plot for (a) fivefold cross validation (R^2 = 0.72; RMSE = 0.282) and (b) prediction results (R^2 = 0.83; RMSE = 0.211) for the anthocyanin concentration models, showing the regression line of the samples (——) the 1:1 trend (——). RMSE, root mean squared error (in mg/g berry).

Discussion

The study presents a solution for the non-destructive, in-field estimation of grape compositional parameters using on-the-go HSI in a vineyard. Specifically, the results support the suitability of hyperspectral cameras for estimating TSS and anthocyanin concentration of grape berries in the field. Until now HSI to assess fruit composition has mostly been conducted in laboratories and indoor environments where the environmental conditions have been controlled, including illumination, temperature, sample positioning and camera stability. Here, the on-the-go hyperspectral images were acquired successfully on a motorised platform at agricultural speeds (5 km/h). The use of a mobile vehicle presents a range of new challenges such as irregularities in terrain and vehicle vibrations, differences in the distance between the lens and the target, and variable speed. The results presented here are, to the best of our knowledge, the first published attempt to automate on-the-go HSI to assess grape composition in the vineyard.

The methodologies studied in this work could be deployed on specific, man-driven platforms (such as the ATV used), other common agricultural vehicles operating upon the crops or even on agricultural robots. This last option would also require an important step of automation in the image computation, something that can be achieved when dealing with hyperspectral images, as the methodology described (the precise selection of grape spectra and the prediction of their composition value) could be directly translated. A collection of grape spectra could be preloaded into the platform's system, limiting the requirement for manual collection of grape sample spectra collection to, for example, once per season. Therefore, along with a pre-trained model, the prediction of grape composition could be fully automated during plot monitoring by the platform. Some previous studies have shown that HSI can be performed under field conditions (Williams et al. 2017) and even on-the-go (Deery et al. 2014, Underwood et al. 2017, Wendel and Underwood 2017). It is possible to integrate HSI sensors, GPS monitoring and computing into a single platform capable of performing real-time assessment in the vineyard and some recent examples of this have been published (Sandino et al. 2018, Vanegas et al. 2018).

Several studies have shown that the monitoring of grape composition throughout ripening is feasible using spectroscopic technologies (Larrain et al. 2008, Cao et al. 2010, González-Caballero et al. 2010, Bellincontro et al. 2011, Barnaba et al. 2014, Musingarabwi et al. 2016) and performed mostly under laboratory conditions. In-field monitoring of grape composition has been reported in previous work using spectroscopy, but from discrete measurements using portable manual devices. A portable NIR spectrophotometer was used for the estimation of TSS under field conditions (Urraca et al. 2016), reporting prediction RMSE values of 1.68°Brix and 10-fold cross validation R^2 up to 0.90 (with an RMSE of 1.47°Brix), with a dataset created

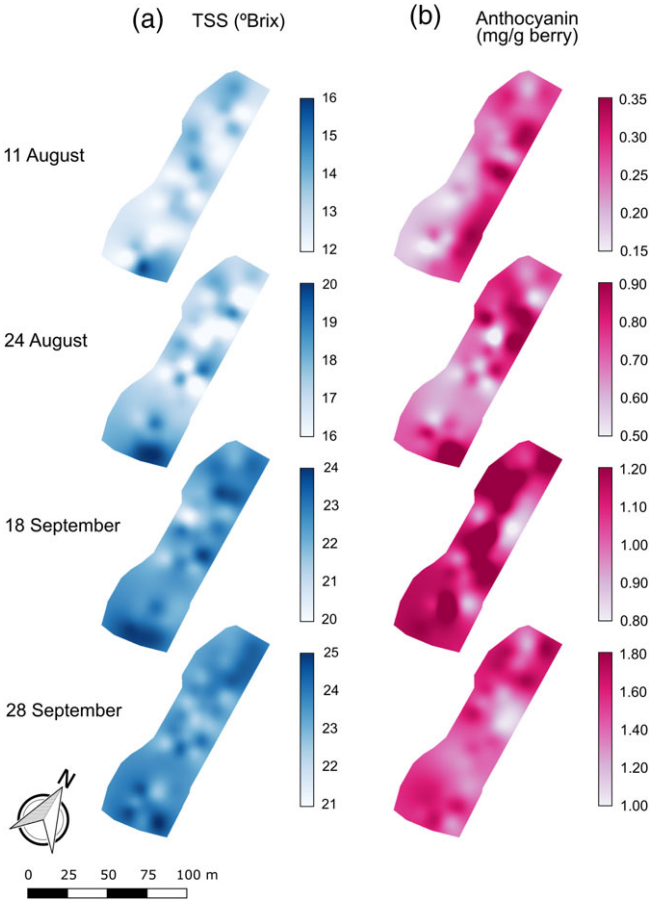

Figure 7. Prediction maps displaying the evolution of (a) TSS and (b) anthocyanin concentration during grape ripening on 11 and 24 August and on 18 and 28 September.

under laboratory conditions. These results are comparable with the results of this study. Furthermore, HSI is an accurate tool for estimation of TSS and anthocyanin concentration under laboratory conditions. Several studies have reported prediction R^2 values from 0.88 to 0.93 (RMSE values of 0.95 and 0.93°Brix, respectively) (Gomes et al. 2017, Piazzolla et al. 2017) for TSS. Importantly, TSS prediction using the on-the-go approach described in this study used the same VIS–NIR spectral region (400–1000 nm). Hyperspectral imaging has been employed to estimate grape anthocyanin concentration (Diago et al. 2016, Martínez-Sandoval et al. 2016, Zhang et al. 2017). The reported R^2 values ranged from 0.72 to 0.93 and are in line with the results presented in this study.

The HSI method developed in this work has overcome two of the three main limitations for on-the-go grape monitoring, that is a larger spot size of measurement (basically all fruit exposed area is measured) and an acceptable signal to noise ratio. The need for fruit to be visible to the sensor still represents a challenge. Partial basal defoliation, however, in the fruiting zone on the side of the canopy exposed to morning sun is a frequent practice in many regions worldwide to improve bunch exposure and air circulation (Smart and Robinson 1991).

The mapping of vineyards to describe spatial variation is a common component of precision viticulture. The technology developed in this study allows the mapping of TSS, anthocyanin concentration and grape ripening spatially in a rapid and non-destructive way (Figure 7).

Conclusions

This study highlights the potential of in-field, on-the-go HSI for the monitoring of grape composition in vineyards. The results obtained from the spectral models trained with support vector machines demonstrate that it is possible to deploy a hyperspectral camera from the laboratory to the field, and that can acquire high resolution information of large areas in a fast, unsupervised manner. An HSI system could be fitted to agricultural machinery or even robotics. Likewise, mapping of grape composition during different phenological stages is possible. This information has the potential to improve winery and vineyard decisions and vineyard management during the season.

Acknowledgements

The project received funding from the European Union under grant agreement number 737669 (Vinescout project). Mr Salvador Gutiérrez would like to acknowledge the research funding FPI grant 299/2016 by Universidad de La Rioja, Gobierno de La Rioja. Dr Maria P. Diago is funded by the Spanish Ministry of Science, Innovation and University with a Ramon y Cajal grant RYC-2015-18429.

References

Baluja, J., Diago, M.P., Goovaerts, P. and Tardaguila, J. (2012a) Spatio-temporal dynamics of grape anthocyanin accumulation in a Tempranillo vineyard monitored by proximal sensing. Australian Journal of Grape and Wine Research **18**, 173–182.

Baluja, J., Diago, M.P., Balda, P., Zorer, R., Meggio, F., Morales, F. and Tardaguila, J. (2012b) Assessment of vineyard water status variability by thermal and multispectral imagery using an unmanned aerial vehicle (UAV). Irrigation Science **30**, 511–522.

Barnaba, F.E., Bellincontro, A. and Mencarelli, F. (2014) Portable NIR-AOTF spectroscopy combined with winery FTIR spectroscopy for an easy, rapid, in-field monitoring of Sangiovese grape quality. Journal of the Science of Food and Agriculture **94**, 1071–1077.

Barnes, R.J., Dhanoa, M.S. and Lister, S.J. (1989) Standard normal variate transformation and de-trending of near-infrared diffuse reflectance spectra. Applied Spectroscopy **43**, 772–777.

Bellincontro, A., Cozzolino, D. and Mencarelli, F. (2011) Application of NIR-AOTF spectroscopy to monitor Aleatico grape dehydration for Passito wine production. American Journal of Enology and Viticulture **62**, 256–260.

Ben Ghozlen, N., Cerovic, Z.G., Germain, C., Toutain, S. and Latouche, G. (2010) Non-destructive optical monitoring of grape maturation by proximal sensing. Sensors **10**, 10040–10068.

Boulton, R.B. (2001) The copigmentation of anthocyanins and its role in the color of red wine: a critical review. American Journal of Enology and Viticulture **52**, 67–87.

Bramley, R.G.V., Le Moigne, M., Evain, S., Ouzman, J., Florin, L., Fadaile, E.M., Hinze, C.J. and Cerovic, Z.G. (2011) On-the-go sensing of grape berry anthocyanins during commercial harvest: development and prospects. Australian Journal of Grape and Wine Research **17**, 316–326.

Cao, F., Wu, D. and He, Y. (2010) Soluble solids content and pH prediction and varieties discrimination of grapes based on visible-near infrared spectroscopy. Computers and Electronics in Agriculture **71**, S15–S18.

Coombe, B.G. (1995) Growth stages of the grapevine: adoption of a system for identifying grapevine growth stages. Australian Journal of Grape and Wine Research **1**, 104–110.

Deery, D., Jimenez-Berni, J., Jones, H., Sirault, X. and Furbank, R. (2014) Proximal remote sensing buggies and potential applications for field-based phenotyping. Agronomy **4**, 349–379.

Diago, M.P., Fernández-Novales, J., Fernandes, A.M., Melo-Pinto, P. and Tardaguila, J. (2016) Use of visible and short-wave near-infrared hyperspectral imaging to fingerprint anthocyanins in intact grape berries. Journal of Agricultural and Food Chemistry **64**, 7658–7666.

Fernández-Novales, J., Tardaguila, J., Gutiérrez, S., Marañón, M. and Diago, M.P. (2017) In field quantification and discrimination of different vineyard water regimes by on-the-go NIR spectroscopy. Biosystems Engineering **165**, 47–58.

Gomes, V.M., Fernandes, A.M., Faia, A. and Melo-Pinto, P. (2017) Comparison of different approaches for the prediction of sugar content in new vintages of whole port wine grape berries using hyperspectral imaging. Computers and Electronics in Agriculture **140**, 244–254.

González-Caballero, V., Sánchez, M.-T., López, M.-I. and Pérez-Marín, D. (2010) First steps towards the development of a non-destructive technique for the quality control of wine grapes during on-vine ripening and on arrival at the winery. Journal of Food Engineering **101**, 158–165.

Huang, L., Zhou, Y., Meng, L., Wu, D. and He, Y. (2017) Comparison of different CCD detectors and chemometrics for predicting total anthocyanin content and antioxidant activity of mulberry fruit using visible and near infrared hyperspectral imaging technique. Food Chemistry **224**, 1–10.

Iland, P., Bruer, N., Edwards, G., Weeks, S. and Wilkes, E. (2004) Chemical analysis of grapes and wine: techniques and concepts (Patrick Iland Wine Promotions: Campbelltown, SA, Australia).

Kennedy, J.A. (2010) Wine colour. Reynolds A.G. , ed. Managing wine quality: viticulture and wine quality (Woodhead Publishing: Cambridge, England) pp. 73–104.

Lamb, D.W., Weedon, M.M. and Bramley, R.G.V. (2004) Using remote sensing to predict phenolics and colour at harvest in a Cabernet Sauvignon vineyard: timing observations against vine phenology and optimising image resolution. Australian Journal of Grape and Wine Research **10**, 46–54.

Larrain, M., Guesalaga, A.R. and Agosín, E. (2008) A multipurpose portable instrument for determining ripeness in wine grapes using NIR spectroscopy. IEEE Transactions on Instrumentation and Measurement **57**, 294–302.

Lee, S., Wolberg, G. and Shin, S.Y. (1997) Scattered data interpolation with multilevel B-splines. IEEE Transactions on Visualization and Computer Graphics **3**, 228–244.

Liang, Z., Wu, B., Fan, P., Yang, C., Duan, W., Zheng, X., Liu, C. and Li, S. (2008) Anthocyanin composition and content in grape berry skin in *Vitis* germplasm. Food Chemistry **111**, 837–844.

Ma, T., Li, X., Inagaki, T., Yang, H. and Tsuchikawa, S. (2017) Non-contact evaluation of soluble solids content in apples by near-infrared hyperspectral imaging. Journal of Food Engineering **224**, 53–61.

Martínez-Sandoval, J.R., Nogales-Bueno, J., Rodríguez-Pulido, F.J., Hernández-Hierro, J.M., Segovia-Quintero, M.A., Martínez-Rosas, M.E. and Heredia, F.J. (2016) Screening of anthocyanins in single red grapes using a non-destructive method based on the near infrared hyperspectral technology and chemometrics. Journal of the Science of Food and Agriculture **96**, 1643–1647.

Meléndez, E., Ortiz, M.C., Sarabia, L.A., Íñiguez, M. and Puras, P. (2013) Modelling phenolic and technological maturities of grapes by means of the multivariate relation between organoleptic and physicochemical properties. Analytica Chimica Acta **761**, 53–61.

Mo, C., Kim, M.S., Kim, G., Lim, J., Delwiche, S.R., Chao, K., Lee, H. and Cho, B.-K. (2017) Spatial assessment of soluble solid contents on apple slices using hyperspectral imaging. Biosystems Engineering **159**, 10–21.

Musingarabwi, D.M., Nieuwoudt, H.H., Young, P.R., Eyéghè-Bickong, H.A. and Vivier, M.A. (2016) A rapid qualitative and quantitative evaluation of grape berries at various stages of development using Fourier-transform infrared spectroscopy and multivariate data analysis. Food Chemistry **190**, 253–262.

Park, B. and Lu, R. (2015) Hyperspectral imaging technology in food and agriculture (Springer: New York, NY, USA).

Pedregosa, F., Varoquaux, G., Gramfort, A., Michel, V., Thirion, B., Grisel, O., Blondel, M., Prettenhofer, P., Weiss, R., Dubourg, V., Vanderplas, J., Passos, A., Cournapeau, D., Brucher, M., Perrot, M. and Duchesnay, E. (2011) Scikit-learn: machine learning in Python. Journal of Machine Learning Research **12**, 2825–2830.

Piazzolla, F., Amodio, M.L. and Colelli, G. (2017) Spectra evolution over on-vine holding of Italia table grapes: prediction of maturity and discrimination for harvest times using a Vis-NIR hyperspectral device. Journal of Agricultural Engineering **48**, 109–116.

Rodríguez-Pulido, F.J., Gil-Vicente, M., Gordillo, B., Heredia, F.J. and González-Miret, M.L. (2017) Measurement of ripening of raspberries (*Rubus idaeus* L.) by near infrared and colorimetric imaging techniques. Journal of Food Science and Technology **54**, 2797–2803.

Rungpichayapichet, P., Nagle, M., Yuwanbun, P., Khuwijitjaru, P., Mahayothee, B. and Müller, J. (2017) Prediction mapping of physicochemical properties in mango by hyperspectral imaging. Biosystems Engineering **159**, 109–120.

Sandino, J., Pegg, G., Gonzalez, F. and Smith, G. (2018) Aerial mapping of forests affected by pathogens using UAVs, hyperspectral sensors, and artificial intelligence. Sensors **18**, 944.

Savitzky, A. and Golay, M.J.E. (1964) Smoothing and differentiation of data by simplified least squares procedures. Analytical Chemistry **36**, 1627–1639.

Smart, R. and Robinson, M. (1991) Sunlight into wine. A handbook for winegrape canopy management (Winetitles: Adelaide, SA, Australia).

Sun, D.-W. (2010) Hyperspectral imaging for food quality analysis and control (Elsevier: San Diego, CA, USA).

Tian, X., Li, J., Wang, Q., Fan, S. and Huang, W. (2018) A bi-layer model for nondestructive prediction of soluble solids content in apple based on reflectance spectra and peel pigments. Food Chemistry **239**, 1055–1063.

Underwood, J., Wendel, A., Schofield, B., McMurray, L. and Kimber, R. (2017) Efficient in-field plant phenomics for row-crops with an autonomous ground vehicle. Journal of Field Robotics **34**, 1061–1083.

Urraca, R., Sanz-Garcia, A., Tardaguila, J. and Diago, M.P. (2016) Estimation of total soluble solids in grape berries using a hand-held NIR spectrometer under field conditions. Journal of the Science of Food and Agriculture **96**, 3007–3016.

Vanegas, F., Bratanov, D., Powell, K., Weiss, J. and Gonzalez, F. (2018) A novel methodology for improving plant pest surveillance in vineyards and crops using UAV based hyperspectral and spatial data. Sensors **18**, 260.

Wendel, A. and Underwood, J. (2017) Illumination compensation in ground based hyperspectral imaging. ISPRS Journal of Photogrammetry and Remote Sensing **129**, 162–178.

Williams, D., Britten, A., McCallum, S., Jones, H., Aitkenhead, M., Karley, A., Loades, K., Prashar, A. and Graham, J. (2017) A method for automatic segmentation and splitting of hyperspectral images of raspberry plants collected in field conditions. Plant Methods **13**, 74.

Zhang, N., Liu, X., Jin, X., Li, C., Wu, X., Yang, S., Ning, J. and Yanne, P. (2017) Determination of total iron-reactive phenolics, anthocyanins and tannins in wine grapes of skins and seeds based on near-infrared hyperspectral imaging. Food Chemistry **237**, 811–817.

Manuscript received: 22 June 2018
Revised manuscript received: 17 August 2018
Accepted: 12 September 2018

Supporting information

Additional supporting information may be found in the online version of this article at the publisher's website: http://onlinelibrary.wiley.com/doi/10.1111/ajgw.12376/abstract.

Table S1. Script of the hyperspectral image analysis algorithm.